

Electronic and magnetic properties of the monolayer RuCl_3 : A first-principles and Monte Carlo study

S. Sarikurt,¹ Y. Kadioglu,² F. Ersan,² E. Vatansever,¹ O. Üzengi
Aktürk,^{3,4} Y. Yüksel,¹ U. Akıncı,^{1,*} and E. Aktürk^{2,4,†}

¹*Dokuz Eylül University, Faculty of Science, Physics Department, Tınaztepe Campus, 35390 zmir, Turkey*

²*Department of Physics, Adnan Menderes University, Aydın 09010, Turkey*

³*Department of Electrical and Electronic Engineering,
Adnan Menderes University, 09100 Aydın, Turkey*

⁴*Nanotechnology Application and Research Center,
Adnan Menderes University, Aydın 09010, Turkey*

(Dated: March 7, 2024)

Recent experiments revealed that monolayer $\alpha\text{-RuCl}_3$ can be obtained by chemical exfoliation method and exfoliation or restacking of nanosheets can manipulate the magnetic properties of the materials. In this present paper, the electronic and magnetic properties of $\alpha\text{-RuCl}_3$ monolayer are investigated by combining first-principles calculations and Monte Carlo simulations. From first-principles calculations, we found that the spin configuration FM corresponds to the ground state for $\alpha\text{-RuCl}_3$, however, the other excited zigzag oriented spin configuration has energy of 5 meV/atom higher than the ground state. Energy band gap has been obtained as 3 meV using PBE functionals. When spin-orbit coupling effect is taken into account, corresponding energy gap is determined to be as 57 meV. We also investigate the effect of Hubbard U energy terms on the electronic band structure of $\alpha\text{-RuCl}_3$ monolayer and revealed band gap increases approximately linear with increasing U value. Moreover, spin-spin coupling terms (J_1 , J_2 , J_3) have been obtained using first principles calculations. By benefiting from these terms, Monte Carlo simulations with single site update Metropolis algorithm have been implemented to elucidate magnetic properties of the considered system. Thermal variations of magnetization, susceptibility and also specific heat curves indicate that monolayer $\alpha\text{-RuCl}_3$ exhibits a phase transition between ordered and disordered phases at the Curie temperature 14.21 K. We believe that this study can be utilized to improve two-dimensional magnet materials.

I. INTRODUCTION

Since the discovery of the graphene,¹ two-dimensional (2D) materials are highly attractive for potential applications in electronic, spintronic and magnetoelectronic devices.^{2–6} The former studies indicate that the low-dimensional materials such as graphene,¹ silicene,⁷ boron nitride,⁸ zinc-oxide,⁹ phosphorene,¹⁰ arsenene,¹¹ antimonene¹² and bismuthene¹³ exhibit a variety of new electronic properties from their bulk phases. In addition to these, investigation of the properties of one- and two-dimensional transition metal chalcogen (TMC) compounds (in the forms of MX_i with $i = 1, 2, 3$ and $\text{X} = \text{O}, \text{S}, \text{Se}, \text{Te}$) has recently received considerable attention because of the fact that the TMCs are generally found to be in three-dimensional (3D) layered structure in which the interlayer is of van der Waals (vdW) type. One of the remarkable properties of these materials which makes them important in nanotechnology is that these TMC compounds have direct energy band gap between 1-2 eV whereas they have indirect energy band gap in 3D phase. The common feature of these aforementioned structures that they are all non-magnetic semiconductor materials. Magnetization can be achieved by doping the material with foreign atoms, generating defects in the material, applying external force or tensile strain.^{14,15} In recent

studies, researchers indicate that it is possible to find 2D materials that have robust intrinsic magnetism. For instance, 2D MnX_2 ($\text{X} = \text{O}, \text{S}, \text{Se}$) materials exhibit ferromagnetism ($3\mu_B$) with Curie temperatures (T_C) 140 K, 225 K and 250 K, respectively.^{16,17} Another group of 3D materials containing transition metals and weak vdW interaction between the layers are metal halides called as MX_3 ($\text{M} = \text{Ti}, \text{V}, \text{Cr}, \text{Fe}, \text{Mo}, \text{Ru}, \text{Rh}, \text{Ir}$ and $\text{X} = \text{Cl}, \text{Br}, \text{I}$). These three-dimensional materials were synthesized years ago.^{18,19} The spacing between the sheets of these materials layered with the ABC packing ranges from 3 to 3.50 Å and is suitable to reduce the dimension from 3D to 2D.²⁰ Hence, in recent years, experimental studies have also been conducted to produce 2D layered forms of metal halogens, and it has been proved that this kind of materials can be experimentally synthesized.²¹

There also exists a rapidly increasing theoretical research activity focused on this area.²² For instance, Liu et al.²³ investigate the ferromagnetism in monolayer Cr-trihalides (CrX_3 ($\text{X} = \text{Cl}, \text{Br}, \text{I}$)) using density functional theory (DFT) combined with the self-consistently determined Hubbard U approach (DFT+ U_{scf}) and Monte Carlo (MC) simulations that based on Ising model. CrBr_3 was obtained as the first ferromagnetic (FM) semiconductor in 1960.²⁴ Liu and coworkers reported that the FM state is always the ground state for CrX_3 (X

= Cl, Br, I) monolayer structures with a net magnetic moment of $6\mu_B$ in each unit cell. Also, they point out that Cr ions give the main contribution to magnetic moment and the neighboring X (X = Cl, Br, I) ions are spin polarized as antiferromagnetic (AFM). They calculate the exchange-correlation energy per unit cell ($E_{ex} = E_{AF} - E_{FM}$) for CrCl_3 , CrBr_3 , CrI_3 as 34, 44 and 55 meV, respectively. These results represent that ferromagnetic (FM) state of each CrX_3 (X=Cl, Br, I) monolayers has the lowest energy and that corresponds to the ground state. So, these monolayer chromium trihalides are reported as a series of stable 2D intrinsic FM semiconductors. CrCl_3 , CrBr_3 , CrI_3 monolayers are semiconductors with energy gap 2.28, 1.76 and 1.09 eV, respectively. Only the interaction between first nearest neighbors was taken into account in the exchange interaction of these monolayer structures and exchange interaction parameters of CrCl_3 , CrBr_3 , CrI_3 obtained as 0.63, 0.81 and 1.02 meV, respectively. The calculated Curie temperature values for CrCl_3 , CrBr_3 , CrI_3 are 66, 86 and 10 K. The Curie temperature values obtained for CrI_3 by different research groups are as follows; 61 K²⁵ and 75 K.²⁶ For CrX_3 (X=F, Cl, Br, I), Zhang et al. have obtained respective Curie temperature such as 41, 49, 73 and 95 K.²⁷ They reported the energy band gap values as 4.68, 3.44, 2.54 and 1.53 eV for CrF_3 , CrCl_3 , CrBr_3 , CrI_3 . According to their calculation results, these 2D Cr-trihalides are half semiconductors with indirect band gaps. For magnetization calculations, they considered the nearest-, next-nearest- and the next-next-nearest neighbor exchange-coupling parameters different from Liu et al.²³ The nearest- and next-nearest-neighbor exchange-coupling parameters are indicated as FM, the next-next-nearest neighbor exchange-coupling parameter as AF for these single layer Cr-trihalides.

He et al.²⁸ obtained the stability, electronic and magnetic properties of VCl_3 and VI_3 monolayers using DFT+ U_{scf} approach together with the MC simulations. Their results represent that VCl_3 and VI_3 monolayers are dynamically stable and also these monolayers exhibit an intrinsic ferromagnetism and half-metallicity. They found that the total magnetic moment per unit cell is $4\mu_B$. According to Heisenberg Hamiltonian, they calculated the nearest-, next-nearest- and the next-next-nearest neighbor exchange-coupling parameters J_1 , J_2 , J_3 as 2.227, 0.144 and 0.02 meV for VCl_3 and 2.754, -0.019 and 0.110 meV for VI_3 , respectively. So, the magnetic interaction of VI_3 single layer structure is greater than VCl_3 . They reported the respective Curie temperature of VCl_3 and VI_3 layers as 80 K and 98 K. They also investigated the effect of the electron and hole doping on ferromagnetism and Curie temperature. The carrier doping leads to an enhancement in ferromagnetism of VCl_3 and VI_3 monolayers. And the Curie temperature of doped VCl_3 and VI_3 increase with increasing the carrier concentration.

The Ruthenium Chloride (RuCl_3) structure known for its interesting catalytic^{29,30} and photochemical³¹ proper-

ties has recently attracted much attention with its magnetic properties. Theoretical and experimental analysis of magnetic and thermodynamic properties for α - RuCl_3 have been examined in many studies.³²⁻³⁸ And besides, the interplay between spin-orbit coupling and electronic correlations have been performed.^{39,40} For the materials with strong spin-orbit coupling (SOC), there exist bond dependent interactions.^{32,41,42} Magnetic properties of these kind of materials can be modeled by the Kitaev-Heisenberg (KH) spin liquid model⁴³ which is defined on a honeycomb lattice. Using this model, field induced magnetization processes in α - RuCl_3 and $A_2\text{IrO}_3$ (A=Na, Li) have been investigated.^{33,41,42} For α - RuCl_3 , KH model has been recently proposed by Banerjee et al.³⁴ In particular, Price and Perkins^{44,45} have performed Monte Carlo simulations based on standard Metropolis algorithm for the investigation of classical KH model. They found that there exists Berezinskii-Kosterlitz-Thouless (BKT) critical behavior before the order-disorder transition takes place.

Most recently, Huang et al.⁴⁶ have calculated the electronic and magnetic properties of RuI_3 monolayer by using spin-polarized DFT and MC simulation. They have obtained the nearest-neighbor exchange-coupling parameter as 82 meV and the Curie temperature approximately $T_C = 360$ K, which is higher than most of the 2D FM nanomaterials studied heretofore. They have also investigated the in-plane strain effect on magnetic exchange and the global band gap of RuI_3 monolayer. Based on the results, they have pointed out that RuI_3 monolayer is an intrinsic FM quantum anomalous Hall insulator. Besides these calculations, they have also analyzed the FM configurations of RuCl_3 and RuBr_3 monolayers. Weber et al. chemically exfoliated the monolayer α - RuCl_3 , but they did not clarify the magnetism of a suspended monolayer on SiO_2/Si substrate.⁴⁷ In another study, Ziatdinov et al. mentioned in their study that magnetic ground state can occur in the geometry of the ligand sublattice in thin films of RuCl_3 .⁴⁸ To the best of our knowledge, the investigation of the possibility of magnetic ground state for α - RuCl_3 monolayer have not been yet thoroughly studied. In this paper, we systematically investigate the electronic and magnetic properties of α - RuCl_3 monolayer using DFT and MC simulations. The magnetic exchange coupling constants have been obtained from DFT calculations. The Curie temperature was calculated by using these exchange-coupling parameters in MC simulations based on the Heisenberg model. The calculated Curie temperature of α - RuCl_3 monolayer is $T_C = 14.21$ K. Our results indicate that monolayer α - RuCl_3 is stable two-dimensional intrinsic ferromagnetic semiconductor.

II. COMPUTATIONAL METHODOLOGY

The calculations for electronic and magnetic properties of α - RuCl_3 have been carried out using DFT with the Projector Augmented Wave (PAW) method^{49,50} as

implemented in the Vienna ab initio Simulation Package (VASP).^{51–54} We have used Generalized Gradient Approximation (GGA) in the Perdew-Burke and Ernzerhof (PBE)^{55,56} form for exchange correlation potential. Furthermore, we investigate SOC effects on the electronic structure of α -RuCl₃. An energy cutoff of 400 eV was used with Gamma-centered Monkhorst-Pack⁵⁷ special k-point grids of $16 \times 16 \times 1$ and $16 \times 8 \times 1$ for bulk α -RuCl₃ and monolayer, respectively. The convergence criterion for total energy is assumed as 10^{-5} eV and the maximum force of 0.002 eV/Å was allowed on each atom. We consider a vacuum layer of about 20 Å thick along the z-axis to eliminate the interaction between neighboring layers. We obtain the phonon dispersion using the finite displacement approach as defined in PHONOPY code⁵⁸ for $2 \times 2 \times 1$ supercell and a displacement of 0.01 Å from the equilibrium atomic positions. To investigate the thermal stability of the optimized α -RuCl₃ monolayer, we performed *ab initio* molecular dynamics (MD) calculations. Verlet algorithm and Nosé thermostat was used for this examination. We also check the structure with Quantum Espresso (QE) software⁵⁹ by using Vanderbilt ultrasoft type pseudopotential. We choose again GGA and PBE parametrisation.

To determine the magnetic structure of α -RuCl₃, the nearest-, next-nearest- and next-next-nearest-neighbors exchange-coupling parameters (J_1 , J_2 and J_3 , respectively), we fit the total energies obtained from DFT calculations for different magnetic configurations to the Heisenberg Spin Hamiltonian:

$$H_{spin} = -J_1 \sum_{ij} S_i S_j - J_2 \sum_{kl} S_k S_l - J_3 \sum_{mn} S_m S_n \quad (1)$$

where S_i is the spin at the Ru site i and (i, j) , (k, l) and (m, n) stand for the nearest, next-nearest and next-next-nearest Ru atoms, respectively. The in-plane ($E[100] - E[010]$) and out-of plane ($E[100] - E[001]$) magnetic anisotropy energies (MAEs) are obtained as 61 μ eV and -18.88 meV, respectively. This negative out-of plane MAE denotes that α -RuCl₃ monolayer has in-plane magnetic anisotropy (in-plane easy axis of magnetization).

By mapping the DFT energies to the Heisenberg Spin Hamiltonian, J_1 , J_2 and J_3 can be calculated from following equations:⁶⁰

$$E_{FM/Neel} = E_0 - (\pm 3J_1 + 6J_2 \pm 3J_3)S^2 \quad (2)$$

and

$$E_{Zigzag/Stripy} = E_0 - (\pm J_1 - 2J_2 \mp 3J_3)S^2 \quad (3)$$

The J_1 , J_2 and J_3 values are found to be 10.69 meV, -1.26 meV and 2.54 meV, respectively. The first and the third neighboring exchange parameters are FM while the second neighboring exchange parameter is AFM. The Curie temperature was calculated by using these exchange-coupling parameters in MC simulations based on the Heisenberg model.

III. MODEL AND DFT SIMULATION DETAILS

α -RuCl₃ has ABC type stacking in layered and has $C2/m$ space group for its bulk form as illustrated in Figure 1. As seen in Figure 1, layered α -RuCl₃ consist of Cl-Ru-Cl sandwich layers and each Ru atom is located at an octahedral site between the Cl atom layers. Therefore while the Cl atoms form a hexagonal pattern, the metal atoms have a honeycomb lattice. Before studying the monolayer form of α -RuCl₃, we first tested the possibility of exfoliation process to obtain monolayer from its bulk form. First, we created bulk α -RuCl₃ with $a=5.99$, $b=10.37$ and $c=6.05$ Å lattice constants as illustrated in Figure 1 (suitable with literature^{47,48,61}) and we implemented a fracture in the bulk after four periodic layer and we systematically increase this fracture distance, at the end we calculate the corresponding cleavage energy (CE) (Figure 1). This method is very effective and has been widely confirmed.^{23,25,27,28} We add separately two van der Waals (vdW) correction terms in the calculations. One of them is the most common used DFT-D2⁶² correction term and the other one is Tkatchenko and Scheffler (TS) method,⁶³ which is formally identical to that of DFT-D2 method. However, in TS method the dispersion coefficients and damping function are charge-density dependent, differently from DFT-D2 method. Obtained CE is 0.174 J/m² for DFT-D2 and 0.238 J/m² for TS correction terms and these energy values are approximately half of the CE of graphite (0.39 ± 0.02 J/m²),⁶⁴ though this energy value can be increase with used vdW correction terms, but we suppose that CE value of α -RuCl₃ will be comparable with those of the other MX₃ (M=Cr, V, Ti; X=Cl, Br, I) materials.^{23,28} Consequently, according to this result α -RuCl₃ monolayer can be obtained by the exfoliation process from its bulk phase whereas realized recently by Weber et al.⁴⁷ Secondly, we obtain the monolayer α -RuCl₃ (see Figure 2(a)), and to confirm the dynamical stability of α -RuCl₃ we calculate the phonon frequencies (see Figure 2(b)) along the main symmetry directions in 2D Brillouin zone (BZ) by using the PHONOPY program, which is based on the finite-displacement method as implemented in VASP.⁵⁸ Our calculations show that there is not any negative frequencies in the BZ, which proved the dynamical stability at $T \sim 0$ K temperature.

In addition, if we see phonon dispersion in more detail, we can see a local minima in the Brillouin zone (at M high symmetry point) for out of plane acoustical branch (ZA). This kind of minima in the phonon bands are associated with Kohn anomalies and cause to discontinuities in $\delta\Omega/\delta k$. In fact, this minima occurs at the high symmetry k-points in the BZ due to singularity of the dielectric function. This situation has been observed in VCl₃, VI₃, NiCl₃, and some MX₂ monolayers.^{28,65,66} In addition, we checked the thermal stability by ab initio MD calculation for 2 ps at 300 K and 700 K, at the end of MD simulations there is not observed any structural deformation, except of small thermal fluctuations.

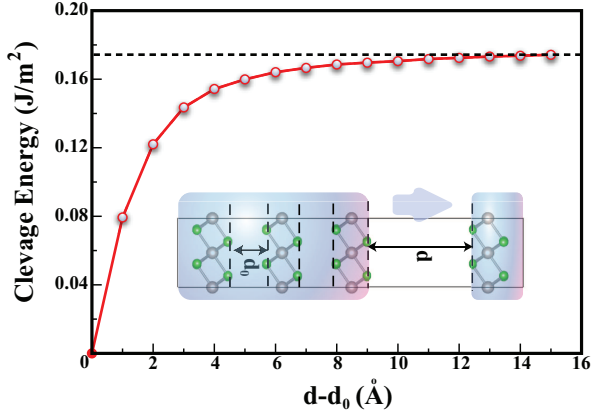


Figure 1. (Color online) Cleavage energy as a function of the separation between two fractured parts. The fracture distance defined as d and the equilibrium interlayer distance of ruthenium trihalides as d_0 . Inside the graph: Side view of bulk α -RuCl₃ used to simulate the exfoliation procedure

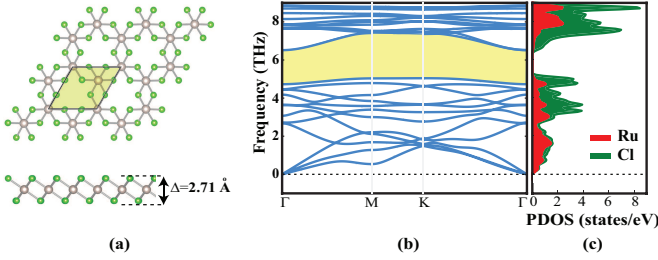


Figure 2. (Color online) (a) Top and side views of the optimized RuCl₃ monolayer (b) Phonon frequencies along the main symmetry directions in 2D Brillouin zone

To determine the favorable magnetic ground state structure of α -RuCl₃, we considered four types of spin configurations (FM, AFM-Néel, AFM-Zigzag and AFM-Stripy) for Ruthenium atoms as shown in Figure 3. We found FM state is the most stable magnetic configuration and RuCl₃ has $4\mu_B$ total magnetic moment (per square unit cell). The other excited configurations, AFM-Néel, AFM-Zigzag and AFM-Stripy have energies higher than the ground state. Relative energy values for other spin oriented systems can be found in S.I Table 1. In this work the electronic band structure and total electronic density of states of FM-RuCl₃ are given in Figure 4. While spin-up channel has large band gap (1.93 eV), spin down channel has almost matching bands between the M and Γ high symmetry points. There is just 3 meV band gap between the valance band maximum (VBM) and conduction band minimum (CBM) for PBE calculation, however these bands are separated from each other and 57 meV band gap occurs with implemented SOC effect in the calculation. Partial density of states (PDOS) are given in Figure 5 to show the contribution of orbital around the Fermi level. As seen in Figure 5 opposite to graphene DOS, p_z does not contribute significantly at

Fermi level for spin-down channel, dominant contribution comes from Ru d-orbital. Two fold e_g (dz^2 and dx^2-dy^2) orbitals and three fold t_{2g} (d_{xy} , d_{yz} and d_{xz}) orbitals give approximately equal contribution to valance bands for both spin-up and -down channels. Cl-p orbitals are dominantly shown at lower energy values than -2 eV. We also checked and confirmed the electronic structure of RuCl₃ by QE and found similar band structure with VASP calculation. Kim et al. found that monolayer α -RuCl₃ shows metallic character by LDA calculation, however it can turn to semiconductor by adding SOC and Hubbard parameter (U) to classical LDA calculation,⁴⁰ and their general trend of band structure is compatible with our band structure. But, unfortunately there is a discrepancy between our band structure and Huang et al. results for RuCl₃.⁴⁶ They found metal for RuCl₃ both of PBE and PBE+SOC calculation and found approximately linear Dirac point at \mathbf{K} high symmetry point, while Kim et al. and Li et al. found band matching between the Γ -M symmetry points.^{40,67} Our result is in fair agreement with Kim et al. and Li et al. As mentioned literature, the electronic and magnetic properties of bulk α -RuCl₃ can be described properly only when a proper Hubbard U term and SOC term is added. Therefore, we investigate the magnetic ground state and electronic properties of single layer RuCl₃ by varying U energy terms. For these calculations we reoptimized the structures to obtain ground state energies for added terms. Relative energies can be found in S.I Figure I, according to our results FM configuration energetically is the most favorable configuration, but for high U values (2.5 eV, 3.0 eV) Zigzag and FM configurations have similar energies, and Neel configurations is the second favorable configuration. Our results also show that band gap of monolayer RuCl₃ has nearly directly proportional with increasing U term, and for $U=1.0$ and 1.5 eV band gaps of FM and Zigzag configured RuCl₃ are approximately 0.27 eV which is similar with experimental result.⁴⁸

IV. MONTE CARLO SIMULATION DETAILS

In order to understand and clarify magnetic properties of the considered α -RuCl₃ monolayer, we use Monte Carlo simulation method with single-site update Metropolis algorithm.^{68,69} The system is located on a $L \times L$ honeycomb lattice, where L is the linear size of the system, and throughout the study we have fixed as $L = 120$. There is a Ru atom in each lattice point in the system. Periodic boundary conditions are applied in all directions. The simulation procedure can be briefly summarized as follows. We note that numerical data are generated over 100 independent sample realizations. In each sample realization, the simulation starts from $T = 30.01$ K using random initial configurations. After, it is slowly cooled down until the temperature reaches $T = 10^{-2}$ K with small temperature steps $\Delta T = 0.2$ K. Spin configurations are generated by selecting the site se-

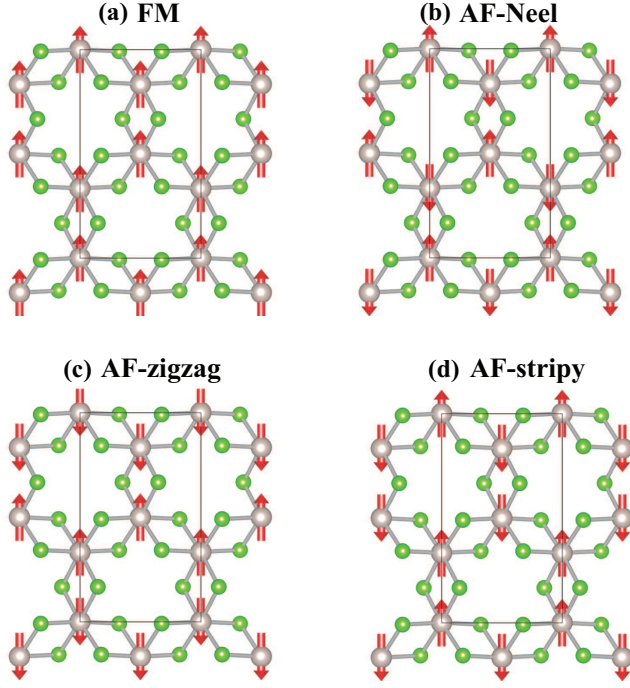


Figure 3. (Color online) Different spin configurations of RuCl₃ monolayer (a) FM ordered (b) AF-Néel ordered (c) AF-Zigzag ordered and (d) AF-stripy ordered.

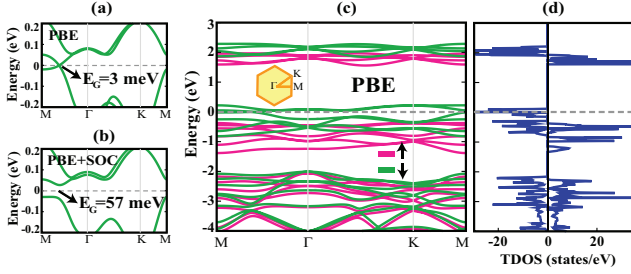


Figure 4. (Color online) Electronic band structure of monolayer RuCl₃ (a) without SOC (b) with SOC. (c) Band structures calculated using PBE functionals and (d) total electronic density of states for monolayer RuCl₃

quentially through the honeycomb lattice. For each temperature, typically first 10^4 Monte Carlo step per site (MCSS) are discarded for thermalization process. Next, 9×10^4 MCSS are used to collect and to determine the temperature dependencies of the physical quantities.

Instantaneous magnetization components of the system can be defined as follows:

$$m_\alpha = \frac{1}{N} \sum_{i=1}^N S_i^\alpha, \quad (4)$$

here N is the total number of the spins in the RuCl₃ monolayer and $\alpha = x, y$ and z . By means of Eq. IV, the magnetization of the system can be given as follows:

$$M = \sqrt{m_x^2 + m_y^2 + m_z^2}. \quad (5)$$

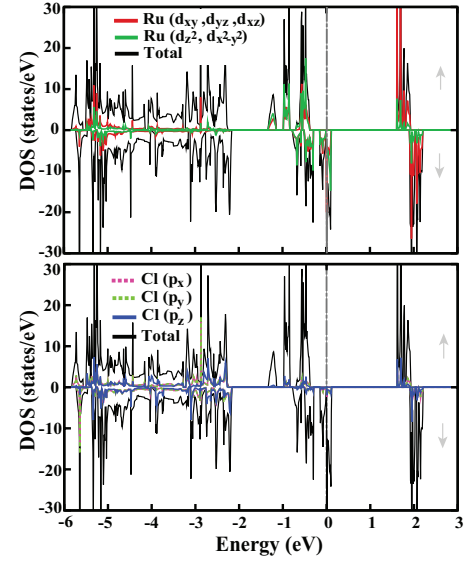


Figure 5. (Color online) The partial and total density of states for the ground states of (a) Ru and (b) Cl atoms of monolayer RuCl₃

In order to determine Curie point of the considered system, we use the thermal variations of the magnetic susceptibility,

$$\chi = N (\langle M^2 \rangle - \langle M \rangle^2) / k_B T, \quad (6)$$

and specific heat curves,

$$C = N (\langle E^2 \rangle - \langle E \rangle^2) / k_B T^2. \quad (7)$$

One can clearly elucidate the magnetic properties of the α -RuCl₃ monolayer using all spin-spin coupling terms and magnetic anisotropy energies, namely J_1 , J_2 , J_3 , k_x and k_y , which are defined in Section II. Thermal variations of magnetization, magnetic susceptibility and specific heat curves are illustrated in Figure 6. Our simulation results suggest that the Curie temperature T_C is 14.21 K. Below this T_C , the α -RuCl₃ monolayer exhibits ferromagnetic character. As shown in Figure 6(a), when the temperature is increased starting from relatively lower temperature value, the magnetization as a function of temperature begins to decrease due to the thermal agitations. Finally, it disappears when the temperature reaches the critical temperature value, and in other words, the system shows a magnetic phase transition between ordered and disordered phases. As displayed in Figure 6(b-c), magnetic susceptibility and specific heat curves display a behavior which tend to diverge as the temperature reaches the Curie temperature. For the sake of completeness, we calculate the specific heat as a function the temperature for the bulk system, as shown in the inset of Fig. 6(c). Spin-spin couplings of the bulk α -RuCl₃ noted in section II are used for this calculation. Note that we followed the same simulation protocol defined for the monolayer α -RuCl₃ because magnetic interlayers are only weakly bonded with the van der

Waals force^{32,34,39}. We know today from the previously published studies⁷⁰ that α -RuCl₃ is antiferromagnetic at the relatively lower temperature regions. Our Monte Carlo simulations support this fact. It is clear from the figure that a phase transition takes place between antiferromagnetic and paramagnetic phases as the temperature reaches the Néel temperature. Our MC simulation results indicate the Néel temperature as $T_N = 10.21$ K, which is in accordance with the previously obtained results ranging from 6.5 K and 15.6 K.^{32,33}

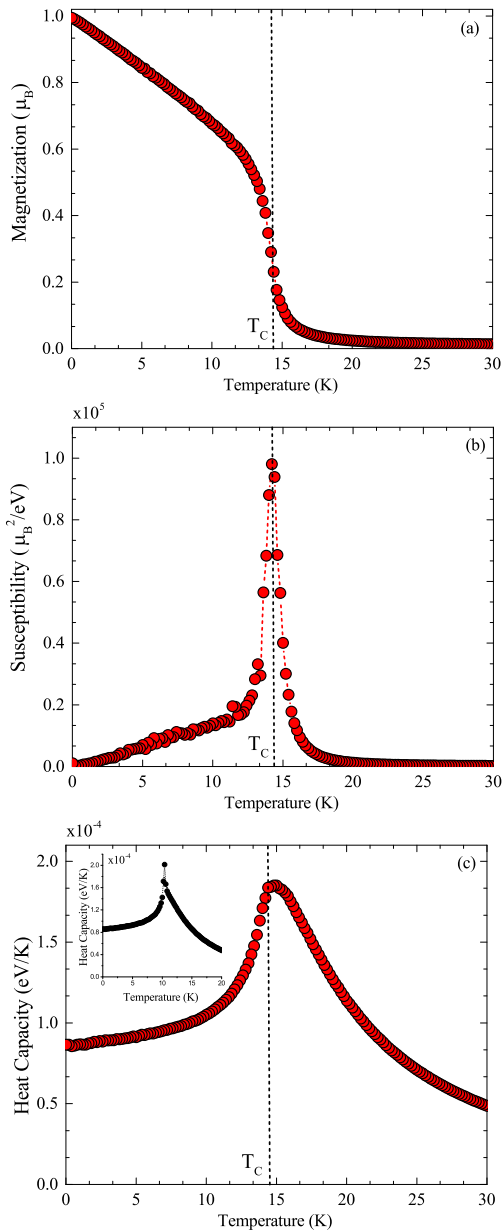


Figure 6. (Color online) (a) Variations of the magnetic moment per site, (b) magnetic susceptibility and (c) specific heat with respect to the temperature. For the sake of completeness, we illustrate the specific heat curve as a function of the temperature of the bulk system in the inset of Fig. 6 (c)

V. CONCLUSIONS

In summary, we used DFT calculations to investigate the stability of RuCl₃ and to determine the electronic and magnetic properties of it. The CE values are smaller than of graphite CE, which means the α -RuCl₃ monolayer can be easily obtained from its bulk phase. According to our DFT calculations, each ruthenium atom gives $1\mu_B$ magnetic moment to the system, so we obtained $4\mu_B$ total magnetic moment for per square cell. Monolayer RuCl₃ has 3 meV band gap around $\Gamma - M$ high symmetry points and this gap increases to 57 meV by adding SOC effect for spin-down channels, while this gap becomes 1.93 eV for spin-up channel. Furthermore, we implemented Monte Carlo simulation based on Heisenberg model to determine temperature dependencies of the magnetic properties of the monolayer α -RuCl₃ system. According to the our simulation findings, present system demonstrate a magnetic phase transition between ordered and disordered phases at the Curie temperature 14.21 K. In addition, we performed an additional Monte Carlo simulation using the same protocol defined for the monolayer to have a better understanding of the behavior the bulk α -RuCl₃ system with respect to the varying temperature. We find that the system shows a phase transition between antiferromagnetic and paramagnetic phases, with the estimated Néel temperature as 10.21 K. We believe that the results obtained in this study would be beneficial for the future theoretical and experimental research on the monolayer α -RuCl₃ system.

VI. ACKNOWLEDGMENTS

his work was supported by the Scientific and Technological Research Council of Turkey (TUBITAK) under the Research Project No. 117F133. Computing resources used in this work were provided by the TUBITAK ULAKBIM, High Performance and Grid Computing Center (Tr-Grid e-Infrastructure).

- * umit.akinci@deu.edu.tr
† ethem.akturk@adu.edu.tr
- ¹ K. S. Novoselov, A. K. Geim, S. V. Morozov, D. Jiang, Y. Zhang, S. V. Dubonos, I. V. Grigorieva and A. A. Firsov, *Science*, 2004, **306**, 666–669
 - ² S. Z. Butler, S. M. Hollen, L. Cao, Y. Cui, J. A. Gupta, H. R. Gutiérrez, T. F. Heinz, S. S. Hong, J. Huang, A. F. Ismach, E. Johnston-Halperin, M. Kuno, V. V. Plashnitsa, R. D. Robinson, R. S. Ruoff, S. Salahuddin, J. Shan, L. Shi, M. G. Spencer, M. Terrones, W. Windl and J. E. Goldberger, *ACS Nano*, 2013, **7** (4), 2898–2926
 - ³ M. Xu, T. Liang, M. Shi and H. Chen, *Chem. Rev.*, 2013, **113** (5), 3766–3798
 - ⁴ M. Chhowalla, H. S. Shin, G. Eda, L.-J. Li, K. P. Loh and H. Zhang, *Nat. Chem.*, 2013, **5**, 263–275
 - ⁵ G. R. Bhimanapati, Z. Lin, V. Meunier, Y. Jung, J. Cha, S. Das, D. Xiao, Y. Son, M. S. Strano, V. R. Cooper, L. Liang, S. G. Louie, E. Ringe, W. Zhou, S. S. Kim, R. R. Naik, B. G. Sumpter, H. Terrones, Y. W. Fengnian Xia, J. Zhu, D. Akinwande, N. Alem, J. A. Schuller, R. E. Schaak, M. Terrones and J. A. Robinson, *ACS Nano*, 2015, **9** (12), 11509–11539
 - ⁶ C. Tan, X. Cao, X.-J. Wu, Q. He, J. Yang, X. Zhang, J. Chen, W. Zhao, S. Han, G.-H. Nam, M. Sindoro and H. Zhang, *Chem. Rev.*, 2017, **117** (9), 6225–6331
 - ⁷ S. Cahangirov, M. Topsakal, E. Aktürk, H. Şahin and S. Ciraci, *Phys. Rev. Lett.*, 2009, **102**(23), 236804
 - ⁸ Z. Zhang and W. Guo, *Nano Letters*, 2012, **12**, 3650–3655
 - ⁹ Z. L. Wang, *J. Phys: Condens. Matter*, 2004, **16**, R829
 - ¹⁰ H. Liu, A. T. Neal, Z. Zhu, Z. Luo, X. Xu, D. Tománek and P. D. Ye, *ACS Nano*, 2014, **8** (4), 4033–4041
 - ¹¹ C. Kamal and M. Ezawa, *Phys. Rev. B*, 2015, **91**, 085423
 - ¹² O. U. Aktürk, V. O. Özçelik and S. Ciraci, *Phys. Rev. B*, 2015, **91**, 235446
 - ¹³ E. Aktürk, O. U. Aktürk and S. Ciraci, *Phys. Rev. B*, 2016, **94**, 014115
 - ¹⁴ Y. Ma, Y. Dai, M. Guo, C. Niu, Y. Zhu, and B. Huang, *ACS Nano*, 2012, **6**(2), 1695–1701
 - ¹⁵ Y. Zhou, Z. Wang, P. Yang, X. Zu, L. Yang, X. Sun and F. Gao, *ACS Nano*, 2012, **6** (11), 9727–9736
 - ¹⁶ M. Kan, J. Zhou, Q. Sun, Y. Kawazoe and P. Jena, *J. Phys. Chem. Lett.*, 2013, **4**(20), 3382–3386
 - ¹⁷ M. Kan, S. Adhikari and Q. Sun, *Phys. Chem. Chem. Phys.*, 2014, **16**(10), 4990–4994
 - ¹⁸ H. Bengel, H.-J. Cantow, S. N. Magonov, H. Hillebrecht, G. Thiele, W. Liang and M.-H. Whangbo, *Surf. Sci.*, 1995, **343**(1), 95–103
 - ¹⁹ H. Hillebrecht, P. Schmidt, H. Rotter, G. Thiele, P. Znnchen, H. Bengel, H.-J. Cantow, S. Magonov and M.-H. Whangbo, *J. Alloys Compd.*, 1997, **246**(1), 70–79
 - ²⁰ Y. Zhou, H. Lu, X. Zu and F. Gao, *Sci. Rep.*, 2016, **6**, 19407
 - ²¹ P. Miró, M. Audiffred and T. Heine, *Chem. Soc. Rev.*, 2014, **43**, 6537–6554
 - ²² M. A. McGuire, *Crystals*, 2017, **7**, 121
 - ²³ J. Liu, Q. Sun, Y. Kawazoe and P. Jenac, *Phys. Chem. Chem. Phys.*, 2016, **18**, 8777
 - ²⁴ I. Tsubokawa, *J. Phys. Soc. Jpn.*, 1960, **15**, 1664–1668
 - ²⁵ M. A. McGuire, H. Dixit, V. R. Cooper and B. C. Sales, *Chem. Mater.*, 2015, **27**(2), 612–620
 - ²⁶ H. Wang, F. Fan, S. Zhu and H. Wu, *EPL*, 2016, **114**(4), 47001
 - ²⁷ W. B. Zhang, Q. Qu, P. Zhu and C. H. Lam, *J. Mater. Chem. C*, 2015, **3**(48), 12457–12468
 - ²⁸ J. He, S. Ma, P. Lyu and P. Nachtigall, *J. Mater. Chem. C*, 2016, **4**(13), 2518–2526
 - ²⁹ M. Fieser, *Fieser and Fieser’s Reagents for Organic Synthesis*, John Wiley & Sons: New York, 1990, vol. 15, p. 280
 - ³⁰ I.-W. Shim, W.-S. Oh, H.-C. Jeong and W.-K. Seok, *Macromolecules*, 1996, **29**(4), 1099–1104
 - ³¹ S. Matsuoka, H. Fujii, T. Yamada, C. Pac, A. Ishida, S. Takamuku, M. Kusaba, N. Nakashima and S. Yanagida, *J. Phys. Chem.*, 1991, **95**(15), 5802–5808
 - ³² J. A. Sears, M. Songvilay, K. W. Plumb, J. P. Clancy, Y. Qiu, Y. Zhao, D. Parshall and Y.-J. Kim, *Phys. Rev. B*, 2015, **91**, 144420
 - ³³ R. D. Johnson, S. C. Williams, A. A. Haghighirad, J. Singleton, V. Zapf, P. Manuel, I. I. Mazin, Y. Li, H. O. Jeschke, R. Valentí and R. Coldea, *Phys. Rev. B*, 2015, **92**, 235119
 - ³⁴ A. Banerjee, C. A. Bridges, J.-Q. Yan, A. A. Aczel, L. Li, M. B. Stone, G. E. Granroth, M. D. Lumsden, Y. Yiu, J. Knolle, S. Bhattacharjee, D. L. Kovrizhin, R. Moessner, D. A. Tennant, D. G. Mandrus and S. E. Nagler, *Nat. Mater.*, 2016, **15**, 733–740
 - ³⁵ T. Aoyama, Y. Hasegawa, S. Kimura, T. Kimura and K. Ohgushi, *Phys. Rev. B*, 2017, **95**, 245104
 - ³⁶ A. U. B. Wolter, L. T. Corredor, L. Janssen, K. Nenkov, S. Schönecker, S.-H. Do, K.-Y. Choi, R. Albrecht, J. Hunger, T. Doert, M. Vojta and B. Büchner, *arXiv preprint arXiv:1704.03475*, 2017
 - ³⁷ L. Janssen, E. C. Andrade and M. Vojta, *arXiv preprint arXiv:1706.05380*, 2017
 - ³⁸ A. Banerjee, J. Yan, J. Knolle, C. A. Bridges, M. B. Stone, M. D. Lumsden, D. G. Mandrus, D. A. Tennant, R. Moessner and S. E. Nagler, *Science*, 2017, **356**, 1055–1059
 - ³⁹ K. W. Plumb, J. P. Clancy, L. J. Sandilands, V. V. Shankar, Y. F. Hu, K. S. Burch, H.-Y. Kee and Y.-J. Kim, *Phys. Rev. B*, 2014, **90**, 041112
 - ⁴⁰ H.-S. Kim, V. V. Shankar, A. Catuneanu and H.-Y. Kee, *Phys. Rev. B*, 2015, **91**, 241110
 - ⁴¹ L. Janssen, E. C. Andrade and M. Vojta, *Phys. Rev. Lett.*, 2016, **117**, 277202
 - ⁴² L. Janssen, E. C. Andrade and M. Vojta, *Phys. Rev. B*, 2017, **96**, 064430
 - ⁴³ A. Kitaev, *Annals of Physics*, 2006, **321**, 2
 - ⁴⁴ C. C. Price and N. B. Perkins, *Phys. Rev. Lett.*, 2012, **109**, 187201
 - ⁴⁵ C. C. Price and N. B. Perkins, *Phys. Rev. B*, 2013, **88**, 024410
 - ⁴⁶ C. Huang, J. Zhou, H. Wu, K. Deng, P. Jena and E. Kan, *Phys. Rev. B*, 2017, **95**, 045113
 - ⁴⁷ D. Weber, L. M. Schoop, V. Duppel, J. M. Lippmann, J. Nuss and B. V. Lotsch, *Nano letters*, 2016, **16**, 3578–3584
 - ⁴⁸ M. Ziatdinov, A. Banerjee, A. Maksov, T. Berlijn, W. Zhou, H. Cao, J.-Q. Yan, C. A. Bridges, D. Mandrus, S. E. Nagler *et al.*, *Nature communications*, 2016, **7**, 13774
 - ⁴⁹ P. E. Blöchl, *Phys. Rev. B*, 1994, **50**, 17953
 - ⁵⁰ G. Kresse and D. Joubert, *Phys. Rev. B*, 1999, **59**, 1758

- ⁵¹ G. Kresse and J. Hafner, *Phys. Rev. B*, 1993, **47**, 558
- ⁵² G. Kresse and J. Hafner, *Phys. Rev. B*, 1994, **49**, 14251
- ⁵³ G. Kresse and J. Furthmüller, *Comput. Mater. Sci.*, 1996, **6**, 15–50
- ⁵⁴ G. Kresse and J. Furthmüller, *Phys. Rev. B*, 1996, **54**, 11169
- ⁵⁵ J. P. Perdew, J. A. Chevary, S. H. Vosko, K. A. Jackson, M. R. Pederson, D. J. Singh and C. Fiolhais, *Phys. Rev. B*, 1992, **46**, 6671
- ⁵⁶ J. P. Perdew, K. Burke and M. Ernzerhof, *Phys. Rev. Lett.*, 1996, **77**, 3865
- ⁵⁷ H. J. Monkhorst and J. D. Pack, *Phys. Rev. B*, 1976, **13**, 5188
- ⁵⁸ A. Togo and I. Tanaka, *Scripta Mater.*, 2015, **108**, 1–5
- ⁵⁹ P. Giannozzi, S. Baroni, N. Bonini, M. Calandra, R. Car, C. Cavazzoni, D. Ceresoli, G. L. Chiarotti, M. Cococcioni, I. Dabo, A. D. Corso, S. de Gironcoli, S. Fabris, G. Fratesi, R. Gebauer, U. Gerstmann, C. Gougoussis, A. Kokalj, M. Lazzeri, L. Martin-Samos, N. Marzari, F. Mauri, R. Mazzarello, S. Paolini, A. Pasquarello, L. Paulatto, C. Sbraccia, S. Scandolo, G. Sclauzero, A. P. Seitsonen, A. Smogunov, P. Umari and R. M. Wentzcovitch, *J. Phys: Condens. Matter*, 2009, **21**, 395502
- ⁶⁰ N. Sivadas, M. W. Daniels, R. H. Swendsen, S. Oakamoto and D. Xiao, *Phys. Rev. B: Condens. Matter Mater. Phys.*, 2015, **91**, 235425
- ⁶¹ H. B. Cao, A. Banerjee, J.-Q. Yan, C. Bridges, M. Lumsden, D. Mandrus, D. Tennant, B. Chakoumakos and S. Nagler, *Physical Review B*, 2016, **93**, 134423
- ⁶² S. Grimme, *J. Comput. Chem.*, 2006, **27**, 1787–1799
- ⁶³ A. Tkatchenko and M. Scheffler, *Phys. Rev. Lett.*, 2009, **102**, 073005
- ⁶⁴ W. Wang, S. Dai, X. Li, J. Yang, D. Srolovitz and Q. Zheng, *Nat. Commun.*, 2015, **6**, 1–7
- ⁶⁵ J. He, X. Li, P. Lyu and P. Nachtigall, *Nanoscale*, 2017, **9**, 2246–2252
- ⁶⁶ C. Ataca, H. Şahin and S. Ciraci, *J. Phys. Chem. C*, 2012, **116**, 8983–8999
- ⁶⁷ W. Wang, Z.-Y. Dong, S.-L. Yu and J.-X. Li, *Phys. Rev. B*, 2017, **96**, 115103
- ⁶⁸ M. E. J. Newman and G. T. Barkema, *Monte Carlo Methods in Statistical Physics*, Oxford University Press: New York, USA, 1999
- ⁶⁹ K. Binder, *Monte Carlo Methods in Statistical Physics*, Springer-Verlag Berlin Heidelberg, 1979
- ⁷⁰ J. M. Fletcher, W. E. Gardner, E. Hooper, K. Hyde, F. Moore and J. Woodhead, *Nature*, 1963, **199**, 1089